LANGMUIR

Article

pubs.acs.org/Langmuir

Velocity Fluctuations in Kinesin-1 Gliding Motility Assays Originate in Motor Attachment Geometry Variations

Henri Palacci,[†] Ofer Idan,[†] Megan J. Armstrong,[†] Ashutosh Agarwal,[†,‡] Takahiro Nitta,[†,§] and Henry Hess*[,†]

[†]Department of Biomedical Engineering, Columbia University, New York, New York 10027, United States

[‡]Department of Biomedical Engineering and Department of Pathology, University of Miami, Coral Gables, Florida 33146, United States

[§]Department of Mathematical and Design Engineering, Gifu University, Gifu 501-1193, Japan

Supporting Information

ABSTRACT: Motor proteins such as myosin and kinesin play a major role in cellular cargo transport, muscle contraction, cell division, and engineered nanodevices. Quantifying the collective behavior of coupled motors is critical to our understanding of these systems. An excellent model system is the gliding motility assay, where hundreds of surface-adhered motors propel one cytoskeletal filament such as an actin filament or a microtubule. The filament motion can be observed using fluorescence microscopy, revealing fluctuations in gliding velocity. These velocity fluctuations have been previously quantified by a motional diffusion coefficient, which Sekimoto and Tawada explained as arising from the addition and removal of motors from the linear array of motors propelling the filament as it advances, assuming that different motors are not equally efficient in their force generation. A computational model of kinesin head diffusion and binding to the microtubule allowed us to quantify the heterogeneity of motor efficiency arising from the combination of anharmonic tail stiffness and varying attachment geometries assuming random motor locations on the surface and an absence of coordination between motors. Knowledge of the heterogeneity allows the calculation of the proportionality constant between the motional diffusion coefficient and the motor density. The calculated value (0.3) is within a standard error of our measurements of the motional diffusion coefficient on surfaces with varying motor densities calibrated by landing rate experiments. This allowed us to quantify the loss in efficiency of coupled molecular motors arising from heterogeneity in the attachment geometry.

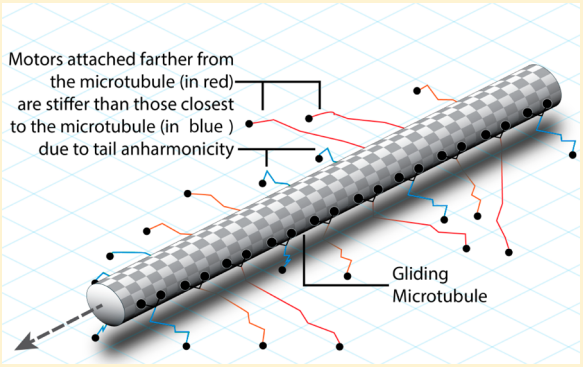

INTRODUCTION

Ensembles of molecular motors are fascinating objects of study in the field of complex dynamical systems because they combine mechanical complexity with chemical stochasticity.[2] The collective behavior of biomolecular motor proteins from the kinesin, dynein, and myosin families and their associated cytoskeletal filaments (microtubules and actin filaments) can be investigated through the construction of in vitro model systems called gliding motility assays where the system dynamics are readily observable by fluorescence microscopy.[4]

In a gliding motility assay, the motor protein's tails are attached to a surface, and their heads bind to a cytoskeletal filament. As the motors step along the filament, the filament is propelled[5] forward. As a result, motors are binding to the tip of the filament and unbinding from its end, thus changing the linear array of motors upon each binding and unbinding event. The elucidation of the dynamics of molecular motors in gliding motility assays has been a goal of theoretical[2,6−15] and experimental efforts[16−18] for 20 years.

Kinesin-1 motor proteins, prominent examples of processive motors,[19] bind to microtubules and execute force-producing steps of constant length d = 8 nm.[20] The number of steps in a given time interval is Poisson-distributed,[21] so the movement of a microtubule propelled by a single kinesin can be characterized by an average velocity v and a diffusive term according to

$$\langle(\Delta X(t) - v\Delta t)^2\rangle = 2D_m\Delta t \quad (1)$$

where $X(t)$ is the position of the filament along its trajectory, $\Delta X(t) = X(t + \Delta t) - X(t)$ is the displacement of the filament during time Δt, and D_m is the motional diffusion coefficient. The motional diffusion coefficient characterizes the fluctuations around the linear velocity of the filament. Measurements with optical tweezers have shown the motional diffusion coefficient D_m to be equal to 1400 nm^2/s for movement driven by individual kinesin-1 motors at saturating ATP concentrations (v

Received: June 24, 2016
Published: July 14, 2016

DOI: 10.1021/acs.langmuir.6b02369
Langmuir 2016, 32, 7943−7950

= 670 nm/s), which is about half of the value of $D_m = vd/2$ = 2700 nm^2/s expected for a Poisson stepper with a step size of d = 8 nm.[21]

When two surface-adhered kinesins are bound to the same microtubule, tracking of the microtubule position with nanometer accuracy has revealed that the microtubule shifts position in increments of one-half of a kinesin step because the low viscous drag on the microtubule leads to a nearly instantaneous sharing of the displacement between the attached motors.[18] However, the steps of the two motors are uncorrelated, and a third motor modifies the microtubule dynamics so that distinct steps cannot be detected anymore.

As the density of surface-adhered kinesins is increased, the average spacing between motors can be reduced all the way to 10 nm,[22] which implies that hundreds of motors interact simultaneously with a microtubule. The mean microtubule velocity has been found to be largely unaffected by the density of kinesin-1 motors, which is expected when the drag on the microtubule is small compared to the force generated by the motors, and the motors do not hinder each other so that they can step at the same velocity as a single unencumbered motor.[23] When a large number of motors are attached, individual steps in the microtubule motion cannot be distinguished.[18] In the limit of many motors, the reduced individual step sizes should lead to a reduction in velocity fluctuations, and for a given motor density, the motional diffusion coefficient should be reduced with microtubule length: indeed, as more motors are attached to the microtubule, the fluctuations should be reduced according to the central limit theorem. However, it has been observed that this is not the case for high kinesin densities.[16] This apparent paradox is resolved by a theoretical analysis by Sekimoto and Tawada,[11] which incorporates the heterogeneity of motor force generation into the analysis of the motion. They conclude that the reduction of velocity fluctuations by the addition of independently acting motors is balanced by an increase in the velocity fluctuations due to the addition and removal of heterogeneous motors from the linear array propelling the filament as it advances.[11] As a result, the motional diffusion coefficient D_m is independent of the length of the microtubule for high kinesin densities.[16] Sekimoto and Tawada's model attributes the heterogeneity of the motors to heterogeneity in their step sizes. However, for kinesin gliding assays, while filament displacement can vary, step sizes are constant at d = 8 nm as a result of the spacing of the tubulin dimers, and their model cannot be directly applied.

Our extension of Sekimoto and Tawada's model to motors with constant step sizes relies on the attribution of the heterogeneity in force production to the anharmonic stiffness of the kinesin tail.[24] The tails of bound motors attached to the surface at a greater distance from the microtubule's axis will tend to have greater stiffnesses and therefore larger force contributions to the shifting force balance between motors as a result of a step (Figure 1). The diffusion coefficient, restating Sekimoto and Tawada's equality in terms of "force-adjusted" step sizes, becomes

$$D_m = \frac{\langle (k_i - \langle k_i \rangle)^2 \rangle}{\langle k_i \rangle^2} \times \frac{v}{2\rho} = \alpha_k \times \frac{v}{2\rho} \quad (2)$$

where k_i is the local stiffness of motor i, ρ is the linear density of motors, and the constant α_k quantifies the heterogeneity of the motor's stiffnesses.

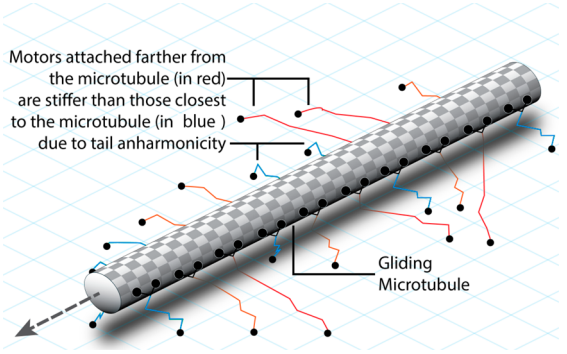

Figure 1. Motors step hand over hand on the microtubule's surface, thus stretching their tail and propelling the microtubule forward. The motors bound farther from the microtubule's axis are stretched more than the bound motors close to the axis. Because the kinesin tail is an anharmonic spring, the stretched motors have a higher force contribution to the forward movement.

Computational models have previously been used to determine the attachment geometry under harmonic potentials,[25] to provide insight into the mechanisms of myosin-coated tracks,[26] or to predict myosin ensemble processivity.[27] Here we modeled the diffusion and binding of the kinesin head under an anharmonic spring potential using Brownian dynamics.[28] This allowed us to determine the spatial distribution of the bound motors as well as the distribution of their tail extension. The force−extension relationship for the kinesin tail then yielded the distribution of bound motor stiffnesses and allowed us to determine a value for the heterogeneity factor α_k of 0.3 (S.E. $\leq$ 0.002).

The spatial distribution of attached motors given by our model also allowed us to determine an effective surface width around the microtubule from which motors bind. This effective width was then used to determine a linear density of bound motors from kinesin surface densities derived from landing rate measurements. Landing rate measurements, in contrast to ellipsometry of quartz crystal microbalance measurements, determine the density of functional motors on the surface (not just the total protein adsorbed).[23,29,30] Combined experimental measurements of the motor surface density, velocity, and motional diffusion coefficient enabled us to determine, for the first time, the constant α in a kinesin/microtubule motility assay for high kinesin densities. A constant α of 0.43 $\pm$ 0.3 SEM (standard error of the mean) was measured; therefore, theoretical and experimental results are in agreement within experimental error. The relatively large error in the experimental determination is primarily a result of the uncertainty in the method used to measure the motor density and cannot be noticeably reduced by analyzing a larger number of gliding filaments.

Determining the origin of velocity fluctuations is a critical step in designing efficient molecular-motor-based nanodevices. We have shown statistical agreement between experimental velocity fluctuation data and our model. Our model links the heterogeneity of force production to the heterogeneity of the attachment geometry. Therefore, the heterogeneity of attachment geometry is a main factor in limiting the energy efficiency of the motor array (S4). Our model can be used in the design of optimized devices, such as motility assays with microfabricated tracks or musclelike actuators with well-aligned motors.

DOI: 10.1021/acs.langmuir.6b02369
Langmuir 2016, 32, 7943−7950

METHODS

Gliding Motility Assays. The experiments were performed at a temperature of 25 °C in approximately 100-μm-high and 1-cm-wide flow cells assembled from two coverslips and double-stick tape.[31] A kinesin construct consisting of the wild-type, full-length *Drosophila melanogaster* kinesin heavy chain and a C-terminal His tag was expressed in *Escherichia coli* and purified using a Ni-NTA column.[32] Microtubules were prepared by polymerizing 20 μg of rhodamine-labeled tubulin (Cytoskeleton Inc., Denver, CO) in 6.5 μL of growth solution containing 4 mM $MgCl_2$, 1 mM GTP, and 5% DMSO (dimethyl sulfoxide) (v/v) in BRB80 buffer (80 mM of PIPES, 1 mM $MgCl_2$, and 1 mM ethylene glycol tetraacetic acid at pH 6.9) for 30 min at 37 °C. The microtubules were then 100-fold diluted and stabilized in 10 μM paclitaxel (Sigma-Aldrich Co., St. Louis MO). The microtubule lengths are Schulz-distributed[33] with an average length of 10.5 μm, a standard deviation of 7 μm, and a minimum length of 3 μm. The same microtubule preparation was used for all kinesin surface densities. The flow cells were first filled with a solution of casein (0.5 mg/mL, Sigma) dissolved in BRB80. After 5 min, it was exchanged with a kinesin solution of concentrations corresponding to motor surface densities of 310 ± 100, 620 ± 200, 1250 ± 400, 2500 ± 790, and 3100 ± 1180 μm^{-2} (all errors are SEM), obtained from landing-rate measurements described previously[29] (S1), in BRB80 with 0.5 mg/mL of casein and 1 mM ATP. After another 5 min, this was exchanged against a motility solution (10 μM paclitaxel, an antifade system made up of 20 mM D-glucose, 20 μg/mL glucose oxidase, 8 μg/mL catalase, 10 mM dithiothreitol, and 1 mM ATP in BRB80) containing 6.4 μg/mL microtubules and was injected for 5 min, followed by two washes with motility solution (without microtubules) to remove excess tubulin. Each flow cell was immediately moved to an epifluorescence microscope (Nikon TE2000), and movies of five different fields of view were taken using a 40× oil objective. The flow cell was imaged every 2 s for 200 s per movie with an exposure time of 200 ms, leading to 100 observations per microtubule. Therefore, a total of 2000 instantaneous velocities for each kinesin densities were obtained. The camera used was an iXON DU885LC (Andor Technology Ltd.) electron-multiplying charge-coupled device (EMCCD). The pixel size on the EMCCD was 8 × 8 μm corresponding to 200 × 200 nm^2 in the object plane.

For each kinesin density, 20 smoothly gliding microtubules were tracked using ImageJ software (NIH), and the tip location was manually determined at every frame. While automated tracking software has made great progress in the past few years,[5,34−36] here the expected gain in accuracy is small because a reduced position measurement error mainly affects the offset in the fluctuation analysis (Figure 4c).

Using MATLAB (Mathworks, Inc.), the distance between two consecutive tip locations, r_j, was measured. The cumulative time interval after i image acquisitions is defined as $\Delta t(i) = i \times \delta t$, where δt = 2 s is the time between image acquisitions. The cumulative distance traveled over the cumulative time interval $\Delta t(i)$, starting at time j, is the sum of single steps $x_j(i) = \sum_{k=j}^{j+i} r_k$, where r_k is the kth distance between tip locations. We therefore obtain, for each trajectory, 100 cumulative distances traveled for a time interval of $\Delta t(1) = \delta t$, 50 cumulative distances traveled for a time interval of $\Delta t(2) = 2\delta t$, and so forth. For each microtubule and time interval, the deviation from the mean cumulative distance traveled, $\Delta x_j(i)$, was calculated as $\Delta x_j(i) = x_j(i) - x_0(i)$, where $x_0(i)$ is the mean cumulative distance traveled over time interval $\Delta t(i)$. The mean square deviation (MSD) for time interval $\Delta t(i)$, $\langle(\Delta x_j(i))^2\rangle = \langle(\Delta x(i))^2\rangle$, was then calculated as an average over all j values of the square deviations over time interval $\Delta t(i)$. We then performed a linear fit of the MSD as a function of the time interval. The diffusion coefficient is related to the slope of this linear fit through the equation

$$\langle(\Delta x)^2\rangle = 2D_m\Delta t + {\sigma_{err}}^2 \tag{3}$$

where ${\sigma_{err}}^2$ is the variance of the distance measurement errors.[16]

The diffusion coefficient for each kinesin concentration was then calculated by averaging the slopes of the linear fits over the 20 microtubules.

To test for the potential length dependence of the velocity fluctuations, we followed Imafuku et al.[16] and fitted the following equation to our experimental data (SI6)

$$D_m(L, \rho) = \frac{kT}{L\varsigma} + D_m(\rho) \tag{4}$$

where L is the length of the filament, ς is the friction coefficient per unit length, k is the Boltzmann constant, T is the temperature, and $D_m(\rho)$ is a length-independent diffusion term. In accordance with Imafuku et al.,[16] we find that the length-dependent term is negligible compared to $D_m(\rho)$ for high kinesin concentrations (kinesin surface densities above 310 μm^2, see SI6). We therefore restricted our analysis to the higher kinesin densities and focused our analysis on $D_m(\rho)$.

To calculate the heterogeneity factor, the linear density of kinesins was calculated on the basis of the surface density

$$\rho = \sigma \times w \tag{5}$$

where w is the effective width of the region on the surface from which kinesins can attach to the microtubule. This width is output from the computational model of kinesin head diffusion and binding to the microtubule (Results section). We find that w = 88 nm. The diffusion coefficient was plotted as a function of the inverse of the linear density, and mean-square regression was used to fit the experimental values to a linear function. The constant α was then calculated according to eq 2 using this linear fit.

Simulating Kinesin Head Diffusion to Determine Attachment Geometry. In order to compute the tail stiffness distribution and linear density of motors from eq 3, we use a Brownian dynamics model of diffusion[28] of the kinesin tail to determine the tail extension distribution and effective binding width. We denote the position of the kinesin head at time t by $\mathbf{r}(t)$ in Cartesian coordinates.

The motion of the kinesin head in each dimension i is given by

$$\frac{dx_i(t)}{dt} = \frac{1}{\zeta}(f_i^k + f^r) \tag{6}$$

where f^k is the elastic force exerted on the diffusing head by the kinesin tail, f^r is the random Brownian force of mean 0 and variance given by

$$\langle f^r(t_1) f^r(t_2)\rangle = 2kT\zeta\delta(t_1 - t_2) \tag{7}$$

where the friction coefficient ζ is given by the Einstein relation for the diffusing tethered kinesin head $D^{kinesin} = kT/\zeta$, δ is the Dirac delta function, k is Boltzmann's constant, and T is the temperature. The value for this diffusion coefficient has been

DOI: 10.1021/acs.langmuir.6b02369
Langmuir 2016, 32, 7943−7950

found to be 20 $\mu m^2/s$, including hydrodynamic effects.[37] We therefore set $D^{kinesin} = 20\ \mu m^2/s$ in the simulations.

The elastic force $\mathbf{f}^k = -f^k\mathbf{r}(t)/\|\mathbf{r}(t)\|$ as a function of tail length at time t, $r(t) = \|\mathbf{r}(t)\|$, was determined on the basis of a numerical inversion of the freely jointed chain (FJC) force–extension relation

$$r(t) = \sum_{i=1}^{n} \coth\left(\frac{f^k l_i}{kT}\right) - \frac{kT}{f^k l_i} \tag{8}$$

where n is the total number of segments i of Kuhn length l_i. The kinesin head has been found to be linked, through a series of five stiffer coiled-coil segments, to its globular tail segment, with a total contour length of 57 nm including the head and tail,[38] thus justifying the freely jointed chain approximation. Here we used for the entropic spring $n = 6$ segments corresponding to the head and freely moving segments between the head and tail with lengths l_i = 8, 15, 10, 5, 6, and 8 nm as specified in ref 38 and considered that the initial tail segment was immobilized on the glass surface. In this model, the tail stiffness exhibits significant nonlinearity, increasing from an initial stiffness on the order of 20 fN/nm to the pN/nm range (Figure 2). The FJC model has been previously used to model tether stiffness[39,40] and fits previous determinations of tether stiffness for low extension.[1,3]

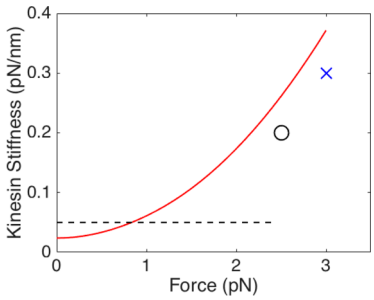

Figure 2. Kinesin-1 tail stiffness as a function of applied force. Red curve: Freely jointed chain model. Black dashed line and circle: approximation of kinesin tail stiffness used by Driver et al.[1] based on their experimental data. Blue cross: approximation of kinesin tail stiffness used by Coppin et al.[3] based on their experimental data. A force of 3 pN is exerted by a fully extended kinesin tail.

We then discretize these equations for a time step of $\Delta t = 0.1\ \mu s$ and run 1000 simulations for a given distance d_{attach} between the microtubule's axis projection on the surface and the kinesin tail's attachment point. We repeat this for d_{attach} taking all integer values between 0 and 50 nm for a total of 5×10^4 simulations. Each simulation stops after the binding event in which the kinesin head reaches the surface of the microtubule, modeled as a 25-nm-diameter cylinder held 17 nm above the surface,[38] or after $t_{max} = 5$ s if no binding event has occurred. We choose this value for t_{max} because initial simulations with longer binding windows showed that only 0.01% of motors have not bonded to the microtubule after 2.5 s (S2). We do not model the unbinding of motors because under our assumptions a completely unbound motor will rebind almost immediately to the microtubule close to the initial binding site (S3 in the Supporting Information). This also ensures that the initial out-of-equilibrium extension energy distribution is preserved over the time scale of binding for one motor.

Modeling the Heterogeneity in Motor Efficiency. In Sekimoto and Tawada's approach,[11] the filament is initially in mechanical equilibrium: the bound motor elastic forces on the microtubule are balanced. Motor i then steps a distance a_i at time t, resulting in a displacement ΔX of the filament to restore mechanical equilibrium. Note that this approximation, and therefore our model, is valid only when the filament is unloaded and in the limit of many motors attached to the filament. Sekimoto and Tawada's original expression for the motional diffusion coefficient is then

$$D_m = \frac{\langle (a_i - \langle a_i \rangle)^2 \rangle}{\langle a_i \rangle^2} \times \frac{v}{2\rho} = \alpha \times \frac{v}{2\rho} \tag{9}$$

where v is the gliding velocity and ρ is the linear density of motors (the inverse of the average spacing), a_i represents the effective step sizes of motor i, and constant α describes the heterogeneity of the motors. A central assumption is that the resistance of the motor to stretching can be described by a spring constant k in the harmonic approximation.

In our approach, the motor step size is fixed at $d = 8$ nm. However, the mechanical equilibrium and thus the filament displacement will depend on motor i's stiffness k_i.

Assuming that motor i steps at time t and that the microtubule's position at time t is $X(t)$, Sekimoto and Tawada's equilibrium condition at t^- (right before the step) and t^+ (right after the step) is

$$\Delta X = X(t^+) - X(t^-) = \frac{a_i}{N} \tag{10}$$

where N is the total number of attached motors and a_i is the step size of motor i. In our model with fixed step sizes and heterogeneous kinesin stiffnesses, the equilibrium condition becomes

$$\Delta X = X(t^+) - X(t^-) = \frac{k_i d}{N\langle k_j \rangle} \tag{11}$$

where d is the 8 nm step size for the kinesin motor and k_i is the stiffness of motor i.

We can therefore, by analogy between eqs 9 and 10, define $\tilde{a}_i = k_i d/\langle k_j \rangle$. Combining this definition of force-adjusted step sizes with eq 8 yields the following expression for the motional diffusion coefficient:

$$D_m = \frac{\langle (k_i - \langle k_i \rangle)^2 \rangle}{\langle k_i \rangle^2} \times \frac{v}{2\rho} = \alpha_k \times \frac{v}{2\rho} \tag{12}$$

Using the simulation results for the distribution of the stiffnesses k_i then allows us to determine the theoretical value of α_k.

RESULTS

Theoretical Determination of the Heterogeneity Factor. The frequency of occurrence of binding at a specific tail extension as a function of the distance d_{attach} between the kinesin surface attachment point and the projection of the microtubule axis on the surface (Figure 3A) was determined using our computational model.

We used this data to estimate the probability of kinesin binding as a function of its horizontal distance from the microtubule axis d_{attach} (Figure 3B). Because of the dramatic increase in the tail stiffness for extensions above 40 nm, the probability of binding within 10 s falls sharply from 100% for d_{attach} = 43 nm to 0% for d_{attach} = 45 nm. This allows us to

DOI: 10.1021/acs.langmuir.6b02369
Langmuir 2016, 32, 7943–7950

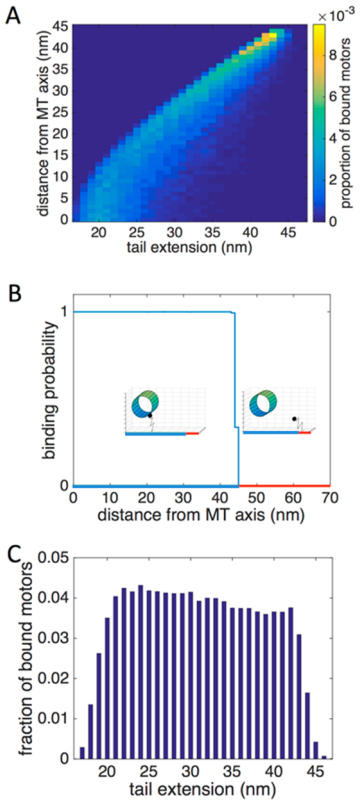

Figure 3. Simulation results. (A) Heat map of motor binding frequency as a function of tail extension and distance d_{attach} from the microtubule axis. (B) Binding probability of surface-adhered kinesins as a function of the distance between the microtubule axis and the kinesin attachment point. (C) Distribution of tail extension over all bound kinesins.

determine a well-defined effective width w = 88 nm to compute the linear density according to eq 4.

We then used the frequency distribution shown in Figure 3A to compute the extension probability distribution $P(r_i)$ = P(extension of kinesin $i = r_i$) over all N bound kinesins (Figure 3C). The force−extension relation for the FJC model in eq 7 links the force f^k to the extension r_i. We can numerically invert this relationship to determine the force distribution $\{f_i^k\}_{i=1\cdots N}$. Numerically differentiating eq 7 with respect to f^k yields a relationship between the force and the local stiffness k_i. We then combine the force distribution with the force−stiffness relationship to compute the distribution of kinesin stiffnesses. Calculating the stiffness distribution's mean and variance allows us to use eq 11 to compute a theoretical value for α_k of 0.3 (SEM ≤ 0.002).

Experimental Measurement of the Heterogeneity Factor. The manual tracking of microtubule tip positions from the fluorescence microscopy images yielded the microtubule trajectories and the time series of velocity fluctuations. The velocity distributions and a discussion of their distance from a normal distribution are discussed in the SI (S5).

The measurements were conducted at a saturating ATP concentration (1 mM) for five different kinesin motor densities ranging from 310 to 3100 μm^{-2}. The lowest kinesin density (310 μm^{-2}) was then excluded from our fit as a result of the length dependence of the motional diffusion coefficient at this kinesin density (S6). The motional diffusion coefficients averaged over 20 microtubule trajectories are shown in Figure 4 first as a function of the motor density (Figure 4A) and then as a function of the calculated inverse of the linear density

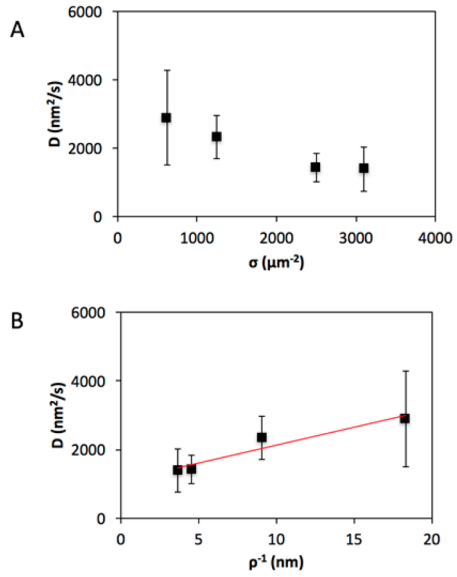

Figure 4. Motional diffusion coefficient as a function of motor density. (A) Motional diffusion coefficient D as a function of kinesin surface density σ. (B) Motional diffusion coefficient D as a function of the inverse of the calculated linear density, ρ^{-1}.

(Figure 4B). We then used the slope of this fit and eq 2 to obtain a value of the heterogeneity factor α of 0.43 ± 0.3 (SEM).

DISCUSSION

Through a computational model of kinesin head diffusion, we were able to estimate the distribution of kinesin tail extensions for kinesins uniformly distributed on a surface and bound to a microtubule. We then combined this distribution and the calculated anharmonic force−extension relation to quantify the theoretical heterogeneity of motor force production. Our model yields a value for the heterogeneity factor α of 0.3 (SEM ≤ 0.002).

By combining measurements of the kinesin surface density and the motional diffusion coefficient, we were also able, for the first time, to determine this heterogeneity factor experimentally. Although Sekimoto and Tawada proposed that the constant is about 1, in our assay a value of 0.43 ± 0.3 (SEM) was found, in good agreement with our theoretical value.

Under our assumptions, we have shown that the variability in the displacement of the microtubule after each motor step can be explained by the variable force contribution of each motor. In our model, each motor has an approximately constant stiffness during its attachment period to the microtubule. This stiffness increases with the distance between the microtubule's axis and the kinesin's attachment point on the surface. This variability leads to heterogeneity in motor force production originating in the heterogeneity in attachment geometry. The asymmetric, highly heterogeneous force production profile is shown in Figure 5.

One of the goals of this study was to observe deviations from the linear dependence of the motional diffusion coefficient on the motor spacing predicted by the model of Sekimoto and Tawada. We expected deviations, especially at high motor densities (small spacings) where increases in the motional

DOI: 10.1021/acs.langmuir.6b02369
Langmuir 2016, 32, 7943−7950

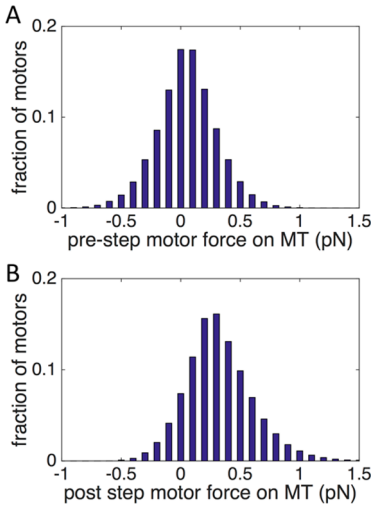

Figure 5. Distribution of forces exerted on the microtubule by the motors along the microtubule axis. (A) Distribution of forces exerted on the microtubule before the step. The average force exerted is 0 pN (by construction). (B) Distribution of the force one motor would exert on the microtubule immediately after it stepped. The average force exerted is 0.3 pN.

diffusion coefficient would indicate increasing correlations between steps. Such stepping cascades have been observed in the gliding of actin filaments on myosin.[41] Kinesin−kinesin cooperation, although relevant when two motors are under load,[24] has not been observed when a large number of kinesins propelled a microtubule whose position was tracked with nanometer resolution.[18] Our measurements, covering a wider range of motor densities, also do not give any indication of a deviation from the expected evolution of the magnitude of the fluctuations. Thus, the Sekimoto−Tawada model (modified to account for the motor distribution on the surface) seems to describe the fluctuations in microtubule gliding on a large number of kinesins in the absence of a large external load concisely. In addition to the heterogeneity in the attachment geometry, which is present with certainty, there are potentially other sources of fluctuations, such as defective motors or motor orientation.[42] Here we carefully selected smoothly gliding filaments to exclude the confounding effect of defective motors. In the case of force-dependent motor unbinding, the fluctuations induced by the unbinding are identical for each motor. Therefore as the length of the microtubule increases, the fluctuations induced by unbinding are averaged out. The diffusion coefficient would then decrease with microtubule length even at high kinesin densities, in contradiction with our experimental results. Therefore all comparable theories explaining fluctuations through factors that are identical across all kinesin motors can be rejected.

Although the original model by Sekimoto and Tawada was formulated for kinesin/microtubule[41] and myosin/actin gliding assays, the results presented here do not translate to the actin/myosin II gliding assay because myosin II is not processive and motor−motor coupling plays a major role.[41] Nevertheless, the impact of heterogeneity in the attachment geometry and non-Hookean tail stiffness[43] may be worth further examination in the actin/myosin gliding assay.

Here, we studied gliding microtubules whose movement is opposed only by viscous drag forces. Velocity fluctuations in a viscous medium will lead to a loss of efficiency on the order of our heterogeneity coefficient (S4). If loads increase, e.g., due to the presence of cargo,[44] then the heterogeneity in force production will prevent the homogeneous distribution of load among motors and thereby will prevent uniform loading with optimal force.[45] This situation is well understood for cargo transport in vivo, where a small number of kinesins collectively pull cargo along microtubules.[24,46,47]

An implication of the above considerations is that obtaining a more uniform attachment geometry via a method to position the motors directly beneath the microtubule,[48] such as that described by Hariadi et al.,[49] would aid the propulsion of the microtubule (Figure 6). A reduction of the track width from 88

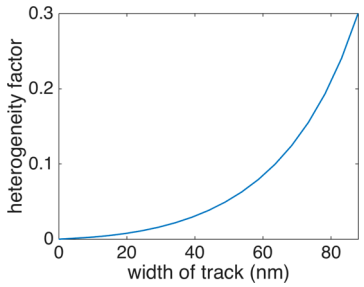

Figure 6. Predicted heterogeneity coefficient as a function of the width of the track the filament is gliding on. As the width of the track goes to 0, the heterogeneity factor is reduced. All track widths greater than 88 nm will display the same heterogeneity coefficient.

to 44 nm would reduce the heterogeneity factor 10-fold. Indeed, muscle, one of the most efficient arrays of molecular motors,[50] features the precise alignment of these motors through the arrangement of thick and thin filaments.

These lessons are instructive for the design of future nanoactuators and molecular-motor-based devices. Although individual components such as kinesin motors may be able to operate with high energy efficiency,[51] the efficiency of arrays and systems may suffer if these components are not appropriately integrated.

■ ASSOCIATED CONTENT

Supporting Information

The Supporting Information is available free of charge on the ACS Publications website at DOI: 10.1021/acs.langmuir.6b02369.

Determination of kinesin densities from landing rate measurements, choice of the time parameter, impact of detachment, loss of efficiency due to fluctuations in a viscous medium, distribution of experimental velocities, and length dependence (PDF)

■ AUTHOR INFORMATION

Corresponding Author

*E-mail: hhess@columbia.edu.

Author Contributions

H.P. and O.I. contributed equally to this publication.

Author Contributions

Conceived and designed the experiments: O.I. and H.H. Performed the experiments: M.J.A., A.A., and O.I. Analyzed the data: O.I., M.J.A., and H.P. Wrote the paper: O.I., M. J.A., H.P., and H.H. Designed and tested the model: H.P., T.N., and H.H. Designed, coded, and operated the simulation: H.P.

DOI: 10.1021/acs.langmuir.6b02369
Langmuir 2016, 32, 7943−7950

Notes

The authors declare no competing financial interest.

■ ACKNOWLEDGMENTS

H.H. thanks Sarah Marzen for helpful discussions. Financial support from the U.S. Army Research Office under W911NF-12-1-0384 and W911NF-13-1-0390 is gratefully acknowledged.

■ REFERENCES

(1) Driver, J. W.; Rogers, A. R.; Jamison, D. K.; Das, R. K.; Kolomeisky, A. B.; Diehl, M. R. Coupling between motor proteins determines dynamic behaviors of motor protein assemblies. *Phys. Chem. Chem. Phys.* **2010**, *12* (35), 10398−10405.
(2) Julicher, F.; Prost, J. Cooperative Molecular Motors. *Phys. Rev. Lett.* **1995**, *75* (13), 2618−2621.
(3) Coppin, C. M.; Pierce, D. W.; Hsu, L.; Vale, R. D. The load dependence of kinesin's mechanical cycle. *Proc. Natl. Acad. Sci. U. S. A.* **1997**, *94* (16), 8539−8544.
(4) Yanagida, T.; Nakase, M.; Nishiyama, K.; Oosawa, F. Direct observation of motion of single F-actin filaments in the presence of myosin. *Nature* **1984**, *307* (5946), 58−60.
(5) Hilbert, L.; Bates, G.; Roman, H. N.; Blumenthal, J. L.; Zitouni, N. B.; Sobieszek, A.; Mackey, M. C.; Lauzon, A. M. Molecular mechanical differences between isoforms of contractile actin in the presence of isoforms of smooth muscle tropomyosin. *PLoS Comput. Biol.* **2013**, *9* (10), e1003273.
(6) Julicher, F.; Ajdari, A.; Prost, J. Modeling molecular motors. *Rev. Mod. Phys.* **1997**, *69* (4), 1269.
(7) Julicher, F.; Prost, J. Spontaneous oscillations of collective molecular motors. *Phys. Rev. Lett.* **1997**, *78* (23), 4510−4513.
(8) Julicher, F.; Prost, J. Molecular motors: From individual to collective behavior. *Prog. Theor. Phys. Suppl.* **1998**, *130*, 9−16.
(9) Tawada, K.; Sekimoto, K. A physical model of ATP-induced actin-myosin movement in vitro. *Biophys. J.* **1991**, *59* (2), 343−56.
(10) Tawada, K.; Sekimoto, K. Protein friction exerted by motor enzymes through a weak-binding interaction. *J. Theor. Biol.* **1991**, *150* (2), 193−200.
(11) Sekimoto, K.; Tawada, K. Extended time correlation of in vitro motility by motor protein. *Phys. Rev. Lett.* **1995**, *75* (1), 180−183.
(12) Sekimoto, K.; Tawada, K. Fluctuations in sliding motion generated by independent and random actions of protein motors. *Biophys. Chem.* **2001**, *89* (1), 95−9.
(13) Duke, T. Cooperativity of myosin molecules through strain-dependent chemistry. *Philos. Trans. R. Soc., B* **2000**, *355* (1396), 529−538.
(14) Duke, T. A. J. Molecular model of muscle contraction. *Proc. Natl. Acad. Sci. U. S. A.* **1999**, *96* (6), 2770−2775.
(15) Imafuku, Y.; Mitarai, N.; Tawada, K.; Nakanishi, H. Anomalous fluctuations in sliding motion of cytoskeletal filaments driven by molecular motors: Model simulations. *J. Phys. Chem. B* **2008**, *112* (5), 1487−1493.
(16) Imafuku, Y.; Toyoshima, Y. Y.; Tawada, K. Fluctuation in the microtubule sliding movement driven by kinesin in vitro. *Biophys. J.* **1996**, *70* (2), 878−86.
(17) Nitta, T.; Hess, H. Dispersion in Active Transport by Kinesin-Powered Molecular Shuttles. *Nano Lett.* **2005**, *5* (7), 1337−1342.
(18) Leduc, C.; Ruhnow, F.; Howard, J.; Diez, S. Detection of fractional steps in cargo movement by the collective operation of kinesin-1 motors. *Proc. Natl. Acad. Sci. U. S. A.* **2007**, *104* (26), 10847−10852.
(19) Howard, J. *Mechanics of Motor Proteins and the Cytoskeleton*; Sinauer: Sunderland, MA, 2001; p 367.
(20) Block, S. M. Kinesin motor mechanics: Binding, stepping, tracking, gating, and limping. *Biophys. J.* **2007**, *92* (9), 2986−2995.
(21) Svoboda, K.; Mitra, P. P.; Block, S. M. Fluctuation analysis of motor protein movement and single enzyme kinetics. *Proc. Natl. Acad. Sci. U. S. A.* **1994**, *91* (25), 11782−6.
(22) Agarwal, A.; Luria, E.; Deng, X. P.; Lahann, J.; Hess, H. Landing Rate Measurements to Detect Fibrinogen Adsorption to Non-fouling Surfaces. *Cell. Mol. Bioeng.* **2012**, *5* (3), 320−326.
(23) Howard, J.; Hudspeth, A. J.; Vale, R. D. Movement of microtubules by single kinesin molecules. *Nature* **1989**, *342*, 154−158.
(24) Berger, F.; Keller, C.; Lipowsky, R.; Klumpp, S. Elastic Coupling Effects in Cooperative Transport by a Pair of Molecular Motors. *Cell. Mol. Bioeng.* **2013**, *6* (1), 48−64.
(25) Arpag, G.; Shastry, S.; Hancock, W. O.; Tuzel, E. Transport by Populations of Fast and Slow Kinesins Uncovers Novel Family-Dependent Motor Characteristics Important for In Vivo Function. *Biophys. J.* **2014**, *107* (8), 1896−1904.
(26) Ishigure, Y.; Nitta, T. Simulating an Actomyosin in Vitro Motility Assay: Toward the Rational Design of Actomyosin-Based Microtransporters. *IEEE Trans. Nanobiosci.* **2015**, *14*, 641.
(27) Egan, P.; Moore, J.; Schunn, C.; Cagan, J.; LeDuc, P. Emergent systems energy laws for predicting Myosin ensemble processivity. *PLoS Comput. Biol.* **2015**, *11* (4), e1004177.
(28) Grassia, P. S.; Hinch, E. J.; Nitsche, L. C. Computer-Simulations of Brownian-Motion of Complex-Systems. *J. Fluid Mech.* **1995**, *282*, 373−403.
(29) Katira, P.; Agarwal, A.; Fischer, T.; Chen, H.-Y.; Jiang, X.; Lahann, J.; Hess, H. Quantifying the performance of protein-resisting surfaces at ultra-low protein coverages using kinesin motor proteins as probes. *Adv. Mater.* **2007**, *19*, 3171−3176.
(30) Dumont, E. L. P.; Belmas, H.; Hess, H. Observing the Mushroom-to-Brush Transition for Kinesin Proteins. *Langmuir* **2013**, *29* (49), 15142−15145.
(31) Howard, J.; Hunt, A. J.; Baek, S. Assay of microtubule movement driven by single kinesin molecules. *Methods Cell Biol.* **1993**, *39*, 137−47.
(32) Coy, D. L.; Wagenbach, M.; Howard, J. Kinesin takes one 8-nm step for each ATP that it hydrolyzes. *J. Biol. Chem.* **1999**, *274* (6), 3667−71.
(33) Jeune-Smith, Y.; Hess, H. Engineering the length distribution of microtubules polymerized in vitro. *Soft Matter* **2010**, *6*, 1778−1784.
(34) Marston, S. Random walks with thin filaments: application of in vitro motility assay to the study of actomyosin regulation. *J. Muscle Res. Cell Motil.* **2003**, *24* (2−3), 149−56.
(35) Scharrel, L.; Ma, R.; Schneider, R.; Julicher, F.; Diez, S. Multimotor transport in a system of active and inactive kinesin-1 motors. *Biophys. J.* **2014**, *107* (2), 365−72.
(36) Ruhnow, F.; Zwicker, D.; Diez, S. Tracking Single Particles and Elongated Filaments with Nanometer Precision. *Biophys. J.* **2011**, *100* (11), 2820−2828.
(37) Leitner, D. M.; Straub, J. E. *Proteins Energy, Heat and Signal Flow*; CRC Press: Boca Raton, FL, 2010.
(38) Kerssemakers, J.; Howard, J.; Hess, H.; Diez, S. The distance that kinesin holds its cargo from the microtubule surface measured by fluorescence-interference-contrast microscopy. *Proc. Natl. Acad. Sci. U. S. A.* **2006**, *103* (43), 15812−15817.
(39) Kierfeld, J.; Frentzel, K.; Kraikivski, P.; Lipowsky, R. Active dynamics of filaments in motility assays. *Eur. Phys. J.: Spec. Top.* **2008**, *157*, 123−133.
(40) Kraikivski, P.; Lipowsky, R.; Kierfeld, J. Enhanced ordering of interacting filaments by molecular motors. *Phys. Rev. Lett.* **2006**, *96*, 25.
(41) Hilbert, L.; Cumarasamy, S.; Zitouni, N. B.; Mackey, M. C.; Lauzon, A. M. The kinetics of mechanically coupled myosins exhibit group size-dependent regimes. *Biophys. J.* **2013**, *105* (6), 1466−74.
(42) Tanaka, H.; Ishijima, A.; Honda, M.; Saito, K.; Yanagida, T. Orientation dependence of displacements by a single one-headed myosin relative to the actin filament. *Biophys. J.* **1998**, *75* (4), 1886−94.
(43) Kaya, M.; Higuchi, H. Nonlinear elasticity and an 8-nm working stroke of single myosin molecules in myofilaments. *Science* **2010**, *329* (5992), 686−9.
(44) Hess, H.; Clemmens, J.; Qin, D.; Howard, J.; Vogel, V. Light-Controlled Molecular Shuttles Made from Motor Proteins Carrying Cargo on Engineered Surfaces. *Nano Lett.* **2001**, *1* (5), 235−239.

DOI: 10.1021/acs.langmuir.6b02369
Langmuir 2016, 32, 7943−7950

(45) Hess, H. Optimal Loading of Molecular Bonds. *Nano Lett.* **2012**, *12* (11), 5813−5814.
(46) Jamison, D. K.; Driver, J. W.; Diehl, M. R. Cooperative Responses of Multiple Kinesins to Variable and Constant Loads. *J. Biol. Chem.* **2012**, *287* (5), 3357−3365.
(47) Uppulury, K.; Efremov, A. K.; Driver, J. W.; Jamison, D. K.; Diehl, M. R.; Kolomeisky, A. B. How the Interplay between Mechanical and Nonmechanical Interactions Affects Multiple Kinesin Dynamics. *J. Phys. Chem. B* **2012**, *116* (30), 8846−8855.
(48) Reuther, C.; Hajdo, L.; Tucker, R.; Kasprzak, A. A.; Diez, S. Biotemplated nanopatterning of planar surfaces with molecular motors. *Nano Lett.* **2006**, *6* (10), 2177−2183.
(49) Hariadi, R. F.; Sommese, R. F.; Adhikari, A. S.; Taylor, R. E.; Sutton, S.; Spudich, J. A.; Sivaramakrishnan, S. Mechanical coordination in motor ensembles revealed using engineered artificial myosin filaments. *Nat. Nanotechnol.* **2015**, *10* (8), 696−700.
(50) He, Z. H.; Bottinelli, R.; Pellegrino, M. A.; Ferenczi, M. A.; Reggiani, C. ATP consumption and efficiency of human single muscle fibers with different myosin isoform composition. *Biophys. J.* **2000**, *79* (2), 945−961.
(51) Wang, W.; Chiang, T. Y.; Velegol, D.; Mallouk, T. E. Understanding the Efficiency of Autonomous Nano- and Microscale Motors. *J. Am. Chem. Soc.* **2013**, *135* (28), 10557−10565.

DOI: 10.1021/acs.langmuir.6b02369
Langmuir 2016, 32, 7943−7950